Contrasting seasonal isotopic signatures of near-surface atmospheric water vapour in the Central Arctic during the MOSAiC campaign

C.F. Brunello [1], H. Meyer [2], M. Mellat [2], M. Casado [3], S. Bucci [4], M. Dütsch [4], M. Werner [1]

[1] Alfred Wegener Institute, Helmholtz Centre for Polar and Marine Research, Bremerhaven, Germany
[2] Alfred Wegener Institute, Helmholtz Centre for Polar and Marine Research, Potsdam, Germany
[3] Laboratoire des Sciences du Climat et de l'Environnement, CEA–CNRS–UVSQ–Paris-Saclay–IPSL, Gif-sur-Yvette, France
[4] Department of Meteorology and Geophysics, University of Vienna, Vienna, Austria

Abstract

The Arctic is experiencing unprecedented moistening which is expected to have far-reaching impact on global climate and weather patterns. However, it remains unclear whether this newly-sourced moisture originates locally from ice-free ocean regions or is advected from lower latitudes. In this study, we use water vapour isotope measurements in combination with trajectory-based diagnostics and an isotope-enabled AGCM, to assess seasonal shifts in moisture sources and transport pathways in the Arctic. Continuous measurements of near-surface vapour, $\delta^{18}O$, and δD were performed onboard RV Polarstern during the MOSAiC expedition from October 2019 to September 2020. Combining this isotope dataset with meteorological observations reveals that the spatiotemporal evolution of $\delta^{18}O$ mimics changes in local temperature and humidity at synoptic to seasonal time scales, while corresponding d-excess changes suggest a seasonal shift in the origin of moisture. Simulation results from the particle dispersion model FLEXPART support these findings, indicating that summer moisture originates from nearby open ocean, while winter moisture comes from more remote sources with longer residence time over sea-ice. Results from a nudged ECHAM6-wiso simulation also indicate that evaporative processes from the ocean surface reproduce summer isotope values, but are insufficient to explain measured winter isotope values. Our study provides the first isotopic characterization of Central Arctic moisture over the course of an entire year, helping to differentiate the influence of local processes versus large-scale vapour transport on Arctic moistening. Future process-based investigations should focus on assessing the non-equilibrium isotopic fractionation during airmass transformation over sea-ice.

Plain language abstract

The Arctic is warming twice as fast as the world´s average and its water cycle is undergoing large changes. The Arctic atmosphere is becoming more humid; however, it is unclear whether the moisture is sourced locally from ice-free ocean regions or if the vapour is transported into the Arctic from lower latitudes. To assess the origin of the moisture, we use the isotopic composition of water vapour obtained onboard a research icebreaker drifting across the Central Arctic ocean. Our observations indicate that the spatial-temporal evolution of $\delta^{18}O$ follows the changes in local temperature and humidity. The corresponding deuterium excess signal, which is used as a diagnostic of moisture source conditions, suggests a seasonal shift in the origin of the air masses. Results from a backward trajectory analyses and from an atmosphere general circulation model indeed show that summer moisture originated from the ocean surface near the sampling site, while winter moisture had a longer residence time over the sea-ice making it more prone to experience isotopic fractionation along the transport. Future model simulations should assess the importance of in-cloud

microphysics and surface moisture exchanges in winter, while additional field observations are needed to reduce the uncertainties on the isotopic data.

Key points

- We present a year of atmospheric water vapour isotopes measurements obtained on a drift cruise across the frozen Central Arctic ocean
- Summer moisture mostly originates from the open ocean and its isotopic composition reflects source region's evaporative conditions
- ECHAM6-wiso cannot reproduce winter moisture´s isotopic composition, suggesting non-equilibrium exchanges during transport over sea-ice

Index terms

3339 ATMOSPHERIC PROCESSES/ Ocean-Atmosphere interactions
3349 ATMOSPHERIC PROCESSES/Polar meteorology
1833 HYDROLOGY/Hydroclimatology
1041 GEOCHEMISTRY/Stable isotope geochemistry
0750 CRYOSPHERE/Sea Ice

Keywords

Water isotopes, atmospheric water vapour, Arctic, water cycle, AGCM

1. Introduction

The Arctic is experiencing a rapid decline of sea-ice coverage and overall alteration of atmospheric and oceanic circulation patterns (Fox-Kemper et al., 2021 in IPCC, 2021). Feedback loops link changes in albedo, water vapour, cloudiness and heat fluxes resulting in an Arctic amplification of the global warming (Holland and Bitz, 2003; Serreze and Barry, 2011; Vihma et al., 2016). Local changes in the Arctic may cause extreme mid-latitude weather events (Cohen et al., 2014) and are also linked to the global climate system by large-scale teleconnections (Huang et al., 2017). Yet the consequences of the changing Arctic remain uncertain due to paucity of observational data and large spread in model projections (Cohen et al., 2020; Ye and Messori, 2021).

Amongst other hydrological changes, a significant increase in the atmospheric specific humidity has been observed in the Arctic in the last two decades (Vihma et al., 2016; Rinke et al., 2019). Whether this additional moisture is locally recycled as a result of an intensified hydrological cycle within the Arctic region itself or is the result of changes in magnitude, distribution and seasonality of regional atmospheric moisture transport, is to date still uncertain. Most studies attribute the moistening of the Arctic atmosphere to northward advection (Zhang et al., 2013). Global warming leads to higher moisture content in the atmosphere and stronger meridional moisture gradients (Bengtsson et al., 2011). Rising temperatures are also expected to cause the poleward migration of the sub-polar westerly jet stream and the intensification of storm-tracks. Hence, more moisture is able to converge into the Arctic region without intensification of the local hydrological cycle. However, conflicting results were reported on the actual frequency of such events in the recent decades (Zahn et al., 2018). In contrast to the advection hypothesis, modelling studies suggest that, under the current warming conditions, the Arctic moisture and consequent precipitation will increase due to intensified local surface evaporation and only to a lesser degree due to enhanced moisture inflow from lower latitudes (Bintanja and Selten, 2014; Bintanja 2018). While the increase of latent heat release in areas of reduced sea-ice extent in winter (Kopec et al., 2016) is undisputed, its contribution was found to be confined to specific regions (Rinke et al., 2019) and seasons (Kurita et al., 2011). Hence, there are doubts on the contribution of surface fluxes on the overall moistening and hydrological sensitivity of the changing Arctic.

Water stable isotopologues ($H_2{}^{16}O$, $HD^{16}O$, $H_2{}^{18}O$, hereafter referred to as water isotopes) are valuable atmospheric tracers because of the various fractionation processes occurring at phase transition and during diffusive vertical vapour transport in the near-surface atmosphere (Urey, 1947). Water bodies that undergo evaporation become enriched in heavy isotopes, while air masses cooling during poleward transport experience depletion due to the removal of heavy isotopes during progressive rainout. Such (a-)diabatic cooling can be described by a Rayleigh model (Craig, 1961). This type of fractionation, dependent on differences in saturation vapour pressure, is referred to as equilibrium fractionation, the strength of which is inversely related to temperature. A different type of fractionation occurs when the phase change is not in equilibrium, such as during evaporation (Dansgaard, 1964; Craig and Gordon, 1965). The difference in diffusion velocity between D/H and $^{18}O/^{16}O$ alters the diffusion rates of the respective water molecules in the air (Merlivat 1978, Hellmann and Harvey 2020). The second-order isotope parameter, deuterium excess (d-excess = $\delta D - 8 * \delta^{18}O$; Dansgaard, 1964), describes the magnitude of such non-equilibrium fractionation.

Stable water isotopes have made significant contributions to deciphering hydroclimatic processes in the Arctic. An important contribution consisted in the attribution of specific isotopic signatures to air masses originating at different latitudes (Bonne et al., 2014,2015,2020; Steen-Larsen et al., 2015;

Leroy Dos Santos et al., 2019). Another area of focus has been on studying the evolution of the isotopic signature of the surface snow during post-depositional processes, which change the isotopic composition of snow through sublimation and solid-condensation (Wahl et al., 2022). This knowledge is not only key for the interpretations of past climate variability in ice-core records; comparisons of measured and modelled water vapour isotopes suggest that snow sublimation in sea-ice covered regions depletes the atmospheric water vapour in $\delta^{18}O$ and increases the d-excess (Bonne et al., 2019). Additionally, d-excess was suggested to be a proxy for sea-ice extent (Klein et al., 2016), due to the coupled strong distillation during the transport and the non-equilibrium evaporative contribution from leads into the atmosphere. Recently, water isotopes have been used to link in-Arctic sourced moisture to extreme snowfall over northern Europe, highlighting a connection between the changing Arctic and the mid-latitude precipitation regimes (Bailey et al., 2021).

Most of the mentioned studies use land-based observations from coastal stations. However, coastlines are not representative for the climate dynamics occurring at higher latitudes where open ocean, sea-ice and snow, co-exist and exchange dynamically through the year. For a long time, the harsh winter conditions, and large extent of concentrated sea-ice had limited ship-based campaigns and fully prevented observations of the winter conditions. This limitation persisted until 2019, when the Multidisciplinary drifting Observatory for the Study of Arctic Climate (MOSAiC) drift experiment (Shupe et al., 2020) offered the unique possibility to address the main hydrological processes occurring in the Central Arctic, covering a complete seasonal cycle including the understudied Arctic winter. From October 2019 to September 2020 the research vessel RV Polarstern (POL) drifted passively across the Central Arctic enabling a cross-disciplinary crew to conduct comprehensive observational and sampling activities. The MOSAiC drift was articulated into five phases, so called 'legs', interjected by personnel rotation, supplies and in some cases active navigation transit for repositioning (Figure 1).

In this study, we investigate the atmospheric water cycle and the moisture source changes during the MOSAiC drifting campaign. We present the first complete annual observation dataset of near-surface atmospheric water vapour isotopes (δD and $\delta^{18}O$) in the Central Arctic. To disentangle local and regional processes, we estimate the atmospheric moisture sources based on Lagrangian backward trajectories. To assess whether climate models successfully capture such local and regional moisture exchange processes, we compare our observations to the results of a simulation from a state-of-the-art atmosphere general circulation model (AGCM) equipped with explicit water isotopes diagnostics and nudged to meteorological analyses.

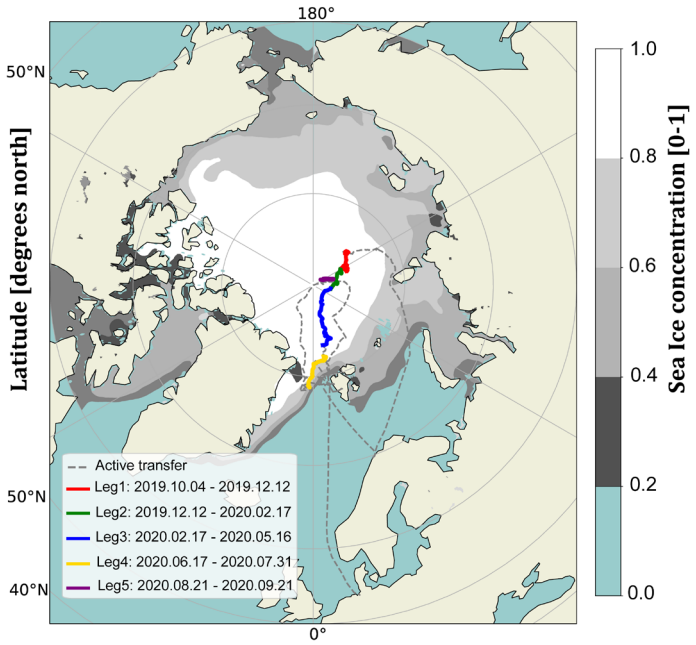

Figure 1: Drift track of RV Polarstern during the Multidisciplinary drifting Observatory for the Study of Arctic Climate (MOSAiC). The total drift is coloured based on the different expedition phases (legs). Active ship movement is illustrated by a grey dashed line. Average sea-ice concentration during the campaign (from ECMWF) is coloured in scale of greys.

2. Data and Methods

2.1 Atmospheric water vapour isotopes

Amongst a large range of other atmospheric observations (Shupe et al. 2022), continuous, in-situ measurements of stable water isotopes were obtained from a Picarro L2140-i CRDS operated during the entire campaign (Brunello et al., 2022a,b,c,d,e). The ambient air inlet was located on the P-Deck, at 29 m above sea level (asl), and connected to the CRDS analyser by a 25 m long stainless-steel tube, heated at 63°C to avoid condensation. The line was pumped with a KNF N 86 KT.18 pump, and the flow rate was about 5 l/min. Raw data of humidity mixing ratio, $\delta^{18}O$ and δD were obtained at the temporal resolution of 1 Hz. The raw isotopic data ($\delta^{18}O$ and δD) obtained from the CRDS were corrected and calibrated using the same custom-made system and correction procedure as described in Bonne et al., 2019. Four different liquid isotopic standards of known isotopic composition were vaporized and injected into the analyser for 30 min every 25 h. Calibration curves were calculated based on the linear regression of the 14-day running average of each standard measurement vs VSMOW and used to correct the ambient measurements. Further, analysers need to be characterized for the response of the measured isotopic values as a function of water vapour concentration. To account for this, prior to the expedition, each isotopic standard besides one, was measured over a range of controlled humidity levels and the results were interpolated with a polynomial function of fourth order (Figure S1). No humidity correction function was available for the most depleted standard. Details about the calibration routine and the empirical corrections can be found in the supplements (Text S1). We found that analytical uncertainties calculated at 1 h resolution are higher during winter, peaking in March (1.1‰, 5.2‰, 10‰, for $\delta^{18}O$, δD and d-excess respectively) and

represent an important, yet unavoidable caveat for this study. Most (84.8%) of the winter (DJFM) observations occurred below 0.4 g/kg, the lowest humidity level for which humidity-response measurements were available (details in Text S2). The entire dataset is presented here, but interpretation of the results at humidity levels below 0.4 g/kg will consider increased uncertainties and when relevant the corresponding data are illustrated with a different marker.

2.2 Meteorological data

The local meteorological data used in this study were routinely measured on POL. The related sensors are located at different heights: relative humidity (RH) and air temperature (T) at 29 m above sea level; air pressure (p) is measured at an altitude of 19 m, but expressed at sea level. Specific humidity (q) is calculated based on RH, T and p. The calibrated and validated datasets are available at a 1-min averaged temporal resolution on PANGAEA (Schmithuesen, 2021).

Gridded near-surface meteorological parameters based on the European Centre for Medium-range Weather Forecasts (ECMWF) fifth-generation reanalysis (ERA5) reanalysis dataset (Hersbach et al., 2023) are used to characterize the spatial sensitivity of the isotope measurements to the environmental conditions during the MOSAiC year. These parameters include single-level variables such as sea surface temperature (SST), 2 m air temperature (T2m), skin temperature (Tskin), surface pressure (SP), 2 m specific humidity (Q2m) obtained from 2 m dewpoint temperature, and sea-ice concentration (SIC). All variables were extracted at 1h resolution. The relative humidity with respect to the skin temperature (RH_{skin}) was calculated as the ratio of specific humidity divided by the saturation specific humidity at skin temperature. Our RH_{skin} is equivalent to the relative humidity with respect to sea surface temperature over the open ocean, however, the use of RH_{skin} allows to extend the calculation over ice-covered regions.

2.3 FLEXPART simulation and moisture source diagnostic

To gain insights into the source regions of sampled water vapour, we used the Lagrangian particle dispersion model FLEXPART (Stohl et al., 2005, Pisso et al., 2019). The model was driven with hourly data from ERA5. Every 3 h, 100,000 atmospheric particles were initialized in a 0.1°×0.1°×100 m box around POL and traced backward for 30 days. The gridded output of this back-trajectory simulation represents the residence time (s) of air masses over the geographic grid cell during their transport. Time series of residence time close to the surface (below 100m altitude, the lowest model output layer) in the last 10 days before arrival were integrated over 6 distinct regional sectors (Asia, Europe, North America, Greenland, open ocean, sea-ice, Figure S2) to show the relative influence of these domains on the atmospheric composition observed at POL year-round.

The backward trajectories were used to identify the source regions of the vapour sampled and measured during MOSAiC based on the diagnostic originally proposed in Sodemann et al. (2008) and subsequently applied on FLEXPART trajectories in Sodemann and Stohl (2009). This moisture source diagnostic is now referred to as WaterSip (Fremme and Sodemann, 2019). WaterSip version 2.8.1 (Bonne et al., 2014) is used to estimate the source regions. The humidity budget of an air parcel is defined as the difference between evaporation (E) and precipitation (P), and WaterSip assumes that at each 3 h time step either E or P dominates while the other can be ignored. Evaporation and precipitation are estimated by integrating the humidity budget (Δq) along each individual trajectory arriving at the position of POL. Increases in specific humidity in the air parcels exceeding the threshold value of 0.1 g kg-1 3h-1 are assumed to result from evaporation, sublimation or

transpiration from the surface, whereas decreases are attributed to precipitation. At each time step, the fractional contribution of a humidity increase is calculated. In case of precipitation, previous evaporation regions are assumed to contribute proportionally to the fraction they represent in the air parcel. When part of the humidity of an air parcel precipitates, all earlier evaporative contributions are thereby reduced accordingly. Eventually, WaterSip provides a fractional contribution of "moisture uptake" (in mm/timestep) on a 0.5°×0.5° grid of each evaporation event to the moisture sampled in the target area. Note that the magnitude of the moisture uptakes depends on the size of the release box. We therefore focus on the relative spatial and temporal differences rather than the absolute variability of the moisture uptakes.

2.4 Water isotope simulation with ECHAM6-wiso

A simulation of the atmospheric water vapour isotope composition was performed with the isotope-enabled atmospheric model ECHAM6-wiso. ECHAM6 is the sixth generation of the atmospheric general circulation model ECHAM, developed at the Max Planck Institute for Meteorology (Stevens et al., 2013). The different water isotopes are treated as inert tracers for atmospheric transport processes in ECHAM6-wiso. Changes of the isotopic composition of an air parcel can thus only occur due to mixing of air masses with different isotopic signatures. Kinetic fractionation processes are included for evaporation of ocean surface water, the formation of snow at low temperatures as well as for the partial re-evaporation of raindrops and snow falling through an undersaturated atmosphere (Cauquoin et al., 2019). Two of the most prominent updates in respect to ECHAM5-wiso (Werner et al., 2011) are related to the isotopic composition of snow-covered sea-ice and the evaporation over ocean, as suggested and parameterized in Bonne et al. (2019). First, the isotopic composition of vapour over sea-ice covered areas is now affected by the isotopic composition of the snow layering on the sea ice surface. Hence, snow sublimation, assumed to happen without fractionation, can deplete the atmospheric water vapour $\delta^{18}O$ and increase the d-excess of the near-surface water vapour. Second, instead of applying the wind speed dependency of the kinetic fractionation factor proposed by Merlivat and Jouzel in 1979, a constant kinetic fractionation factor is applied (Benetti et al., 2014).

In this study, we present the results from a single model simulation performed at a horizontal grid size of ∼0.9×0.9° and 95 vertical levels (T127L95). To ensure that the simulated large-scale atmospheric flow is modelled in agreement with the ECMWF reanalysis data, the model is nudged to ERA5 surface pressure, temperature, vorticity and divergence fields (Butzin et al., 2014). For each model output time step (6 h), the simulated water vapour amount and its isotopic composition are extracted from the near-surface model grid cell encompassing the position of POL along the MOSAiC drifting track. In the vertical direction, this near-surface grid cell extends from the surface to ∼60 m above the surface.

3. Results

In the following section, we present the results of our investigation of atmospheric stable water isotopes measured during the MOSAiC expedition in the central Arctic Ocean. It is important to note that the observed changes are not solely driven by seasonal variations; they also reflect fluctuations caused by the drifting cruise and relocations of RV Polarstern (POL). Therefore, the patterns we discuss are the combined result of both spatial and temporal factors. Throughout this manuscript,

the significance of the correlation analyses is assessed using p-values. Unless stated otherwise, all correlations reported in this study have p-values below 0.01.

3.1 Water vapour isotope variations at RV Polarstern during the MOSAiC expedition

The calibrated data of water vapour $\delta^{18}O$ and δD from the Picarro CRDS, and the related time series of specific humidity (q) and air temperature (T) measured routinely as part of the meteorological observations on POL are displayed in Figure 2.

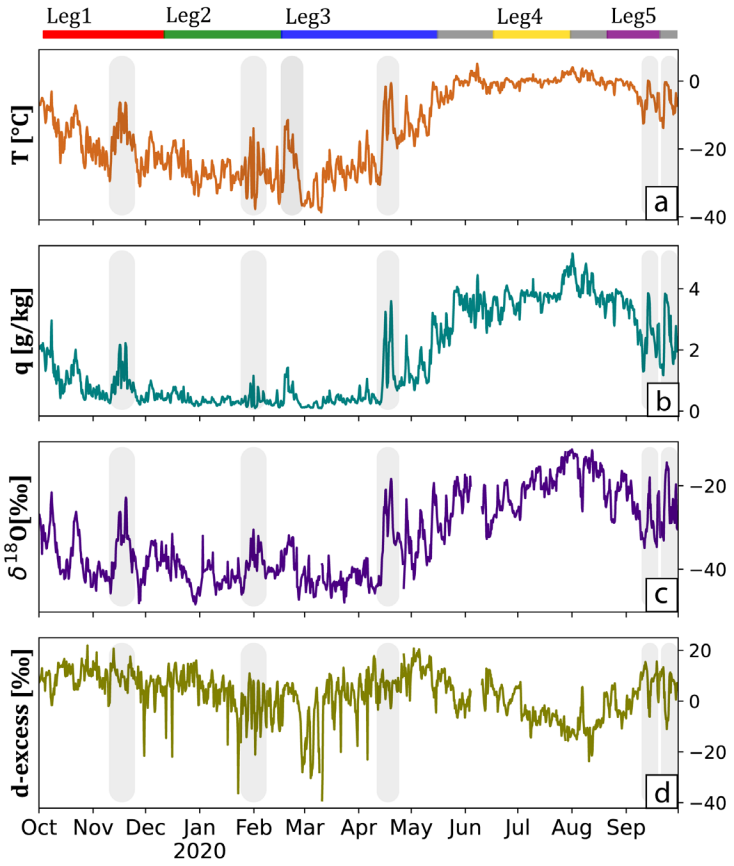

Figure 2: From top to bottom: (a) temperature, (b) humidity, (c) $\delta^{18}O$, and (d) d-excess of atmospheric water vapour measured at 19m on the mast of RV Polarstern during the MOSAiC drifting expedition in the Central Arctic, aggregated here at 6 h resolution. The time span of each phase of the expedition (named legs, Fig.1) is illustrated in the upper bar, the active transfer of RV Polarstern is shown as a grey phase. Vertical shaded grey bars in panels (a)-(d) mark the occurrence of synoptic warm air intrusions.

The dataset spans from October 1st, 2019 to September 30th, 2020 and includes a total of 7564 hourly data points, accounting for 86% of a full annual cycle. Gaps in the water isotope data exist due to the removal of outliers related to instable measurements of the Picarro instrument (details in S1). Furthermore, vapour data were not collected from June 03 to June 08 when POL entered the Svalbard territorial waters and atmospheric measurements were not permitted.

Aggregated to a 3 h resolution, temperature and humidity values over the course of the MOSAiC expedition year range between -38.8 °C to 5.2 °C (mean: -14.3 °C, std: 11.8 °C) and 0.1 g/kg to 5.1 g/kg (mean: 1.7 g/kg, std: 1.4 g/kg), respectively. The $\delta^{18}O$ dataset ranges from a minimum of -49‰

to a maximum of -11.3‰ (mean: -32.3‰, std: 9.7‰), while the d-excess data series spans a wide range of values, with a minimum of -46.5‰ and a maximum of 24.5‰ (mean:2.5‰, std:8.9‰).
Temperature, specific humidity, and $\delta^{18}O$, show a seasonal cycle in the data series, with low values in the boreal winter (December–March) and high values during the boreal summer (June–September). The seasonal changes of these three variables are correlated. On the opposite, no clear seasonal cycle is observed for the d-excess values, which show a high variability throughout the entire winter time and a decreasing trend from May to September, in antiphase with the summer $\delta^{18}O$ values.
Several positive $\delta^{18}O$ excursions are observed on a sub-seasonal, synoptic time scale, coinciding with maxima in both local temperature and specific humidity (Figure 2, vertical grey bars). Most of these excursions can be identified as the local expression of warm intrusions carrying moist air masses from mid-latitudes poleward into the Central Arctic (Rinke et al. 2019). These events are more noticeable in winter and autumn. Typically, such passage of extratropical cyclones and their associated warm (cold) sectors leads to positive (negative) anomalies of $\delta^{18}O$ in anticorrelation with changes in d-excess (Dütsch et al., 2016, Thurnherr et al., 2021). In all cases of our data set, warm air intrusions led indeed to an increase in $\delta^{18}O$ and a matching decrease in d-excess, except for the events in December and February, where the d-excess values were increasing, too. In addition, extreme negative d-excess excursions with no counterpart of positive $\delta^{18}O$ changes are observed both in wintertime (with strongest negative excursions between mid-February and mid-March) and summertime (July and August). No daily cycles were observed at any time during the observational period, neither in the vapour isotopic composition nor in the air temperature and humidity. The lack of diurnal variability implies that the moisture measured on board POL is not influenced by diurnal changes in local radiation, surface fluxes and boundary layer mixing and that the synoptic and seasonal changes dominate the records.

3.2 Linking RV Polarstern vapour data with regional surface temperature and humidity changes

In order to explore the linkage of the water vapour isotopes to environmental variables at the regional scale, correlation analyses were conducted using the gridded meteorological reanalysis data from ERA5. These maps are especially relevant for the identification of evaporative source regions, which might differ from the conditions at the sampling site. While variations in surface temperature lead to changes in evaporation from water bodies influencing the $\delta^{18}O$ composition, relative humidity with respect to surface temperature is a driving factor for kinetic fractionation (Pfahl and Wernli, 2008). Figure 3 shows seasonal mean correlation values of $\delta^{18}O$ with T_{skin} and d-excess with RH_{skin}, respectively.
During summer, the water vapour $\delta^{18}O$ variations correlate positively with T_{skin} over the open ocean (Fig. 3a). These correlations are spatially unselective and cover most of the ocean sector, which indicates that seasonal temperature changes in the Arctic are spatially coherent for most regions. An opposite, but weaker correlation is found in the mixed sea ice-open ocean sector north of Alaska and Siberia. Correlation values over the sea-ice area are low and largely non-significant as opposed to winter (Fig. 3c), where a positive correlation pattern is observed over the frozen Central Arctic Ocean. The summer d-excess variations correlate negatively with the RH_{skin} over the Central Arctic Ocean (Fig. 3b), with the highest values found in the Greenland Sea, straddling the margin of the sea-ice. Positive correlation is observed over the open ocean along the Siberian coast and Bering Strait.

Positive significant correlation is also found between d-excess and RH_{skin} over the sea-ice in winter (Fig. 3d), although correlation values are low and without a consistent spatial pattern. Low correlation is also observed in the Atlantic Ocean, Scandinavia and Bering Strait.

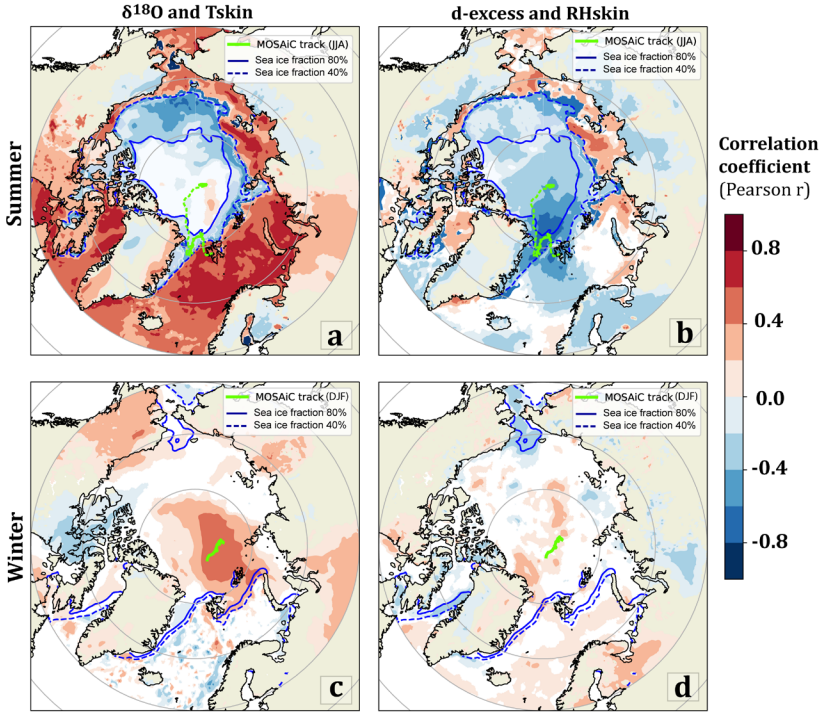

Figure 3: Seasonal correlation maps (Pearson's r at 99.9% confidence interval) of water vapour $\delta^{18}O$ and skin temperature Tskin (a,c) and d-excess and relative humidity RHskin (b,d). Panels a and b show the Arctic summer (JJA), c and d the winter season (DJF). The blue lines mark the area of sea fraction higher than 80% (solid) and 40% (dashed), respectively. Correlation coefficients were calculated based on the 3 h resolution data sets at all locations north of 60°N, assuming no time lag.

These results suggest distinct moisture sources for summer and winter conditions. In summer, the strong positive correlation between $\delta^{18}O$ in vapor and temperature variations over the ice-free North Atlantic and Barents Sea suggests moisture uptake from these regions. Additionally, d-excess indicates that especially uptake from the sea-ice margin plays a role in modulating the non-equilibrium fractionation of summer moisture. In contrast, during winter, water vapour $\delta^{18}O$ and d-excess, correlates primarily with temperature and humidity changes over sea-ice-covered areas. This may suggest either a contribution from locally recycled moisture or a superposition of the primary oceanic evaporation signal by additional fractionation processes during the transport of vapour over sea-ice in winter. However, the complex correlation patterns of d-excess do not allow more precise conclusions here.

3.3 Trajectory-based moisture source diagnostic

In order to further investigate the influence of changes in moisture source regions on the isotopic composition of the water vapour, we applied a moisture source diagnostic to the backward air trajectory simulations obtained from the FLEXPART atmospheric transport model. Note that the

absolute values are low as they represent the contribution of the moisture content within a small release box (Sec. 2.3).

The average moisture uptake in millimetres per day for each calendar season, is illustrated in Figure 4. Our findings show that the moisture sources of the vapour measured at POL during the MOSAiC campaign varied from season to season, both in location and strength (Fig. 4a, b). Strong evaporation from different source regions associated with short residence times is taking place in summer (June-Aug) and low evaporation associated with longer residence times in the late winter (Feb-April). These seasonal differences in evaporation strength are reflected in the corresponding variations in specific humidity at POL (Fig. 2).

With regard to the key moisture source regions, in autumn, at the beginning of the MOSAiC expedition, predominantly moisture from the Arctic Ocean was transported to POL (Fig. 4c). Three main source regions could be identified: (i) the area surrounding POL, which is fully covered by sea-ice; (ii) the sea-ice margin over the Laptev, Eastern Siberian and Beaufort Seas, where sea-ice concentration is on average lower and mixed conditions of open ocean and growing sea-ice can be found and (iii) the ice-free Barents Sea. In winter, the overall moisture uptake decreases, the uptake over sea-ice covered areas vanishes and the only remaining moisture source is the ice-free Barents Sea (Fig. 4d). During spring, while POL drifted southward across the Arctic Ocean, moisture uptake increased again and the moisture uptake region extended from the Barents Sea westward to Svalbard and the Greenland Sea (Fig. 4e). This shift might be partly also caused by the more southern position of POL. This season marks a transition from winter conditions with large sea-ice areas to melting conditions with retreating sea-ice areas. In summer, moisture uptake is at its seasonal maximum (ca. 0.017 mm d^{-1}). The moisture source region covers a large sector of the Arctic ocean, with the most prominent contribution from the southern and western coasts of Svalbard, surrounding POL. Additional contribution is provided from the Central Arctic and the Eurasian coastal regions. The wide distribution of moisture sources can be attributed both to warmer temperature and larger availability of liquid water, and to the spatial variability in sampling, due to the relocation of POL from Leg 4 to Leg 5 (Fig.1). In Figure S3, we present the moisture uptakes of each Leg separately. Both Leg 4 and 5 experienced large spread in moisture source locations with significant contribution from the open ocean. However, during Leg 4, POL primarily received moisture from the west of Svalbard, whereas during Leg 5, the majority of the moisture originated from the Laptev Sea. These two patterns combine to form the average summer (JJA) moisture uptake map.

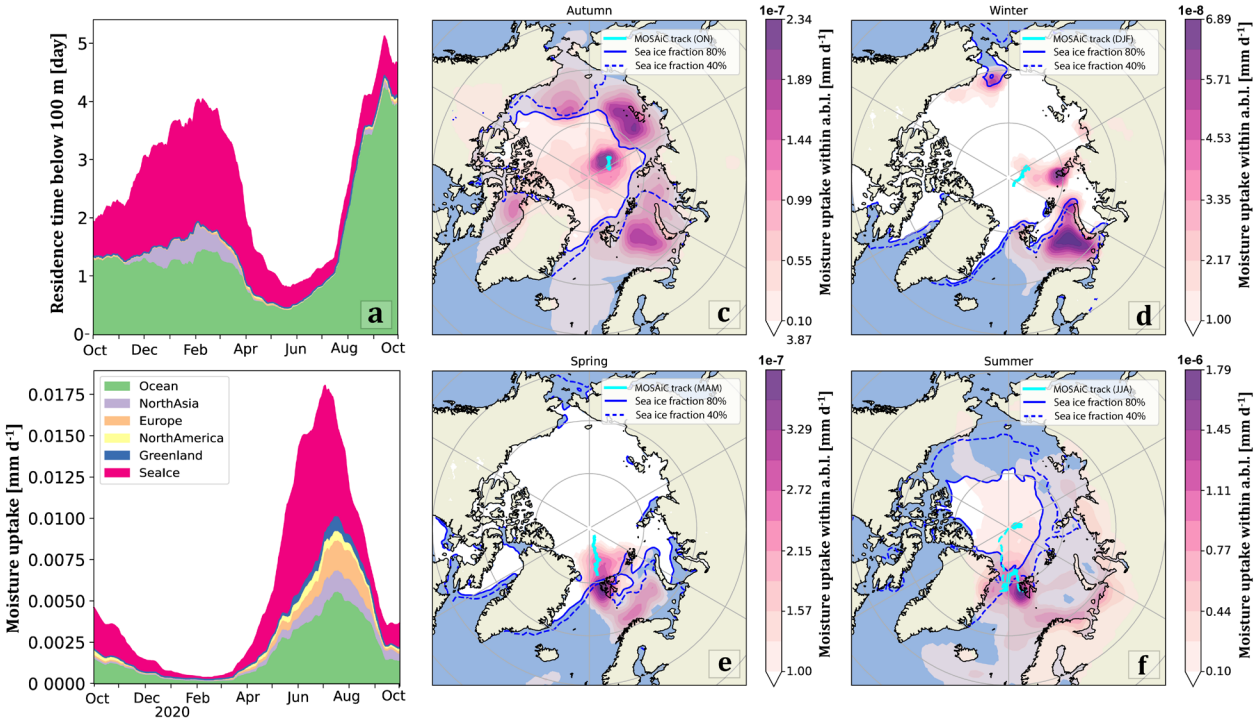

Figure 4. Left panels: 60-day running average of (a) residence time below 100 m obtained from the FLEXPART model and (b) moisture uptake under the atmospheric boundary layer (a.b.l) from the WaterSip diagnostic, computed along the MOSAiC track and aggregated over distinct regions. Right panels: regional maps with seasonal averages of boundary layer moisture uptake (mm d^{-1}). The solid cyan line marks the seasonal track of RV Polarstern, the blue lines mark the area of sea-ice fraction higher than 80% (solid) and 40% (dashed).

3.4 Comparison of RV Polarstern measurements with ECHAM6-wiso simulation results

To gain further understanding of the observed isotopic changes, and to assess whether an AGCM reproduces these changes, we compare the isotopic and meteorological observations from MOSAiC (Fig. 2) with model results from a nudged ECHAM6-wiso atmospheric simulation (Sec. 2.4).

The modelled air temperature changes (Fig 5a) match closely the observations (r^2=0.94) because in this ECHAM6-wiso simulation the modelled 3D-field of temperature was nudged toward ERA5 reanalysis data every 6 h. In contrast, none of the hydrological variables in the ECHAM model were nudged, to allow a physically consistent interpretation of the simulated water vapour isotope values. Nevertheless, simulated humidity changes (Fig 5b) are in very good agreement with the observations as well (r^2=0.96). This is true for both the mean levels, and on a seasonal and synoptic time scale.

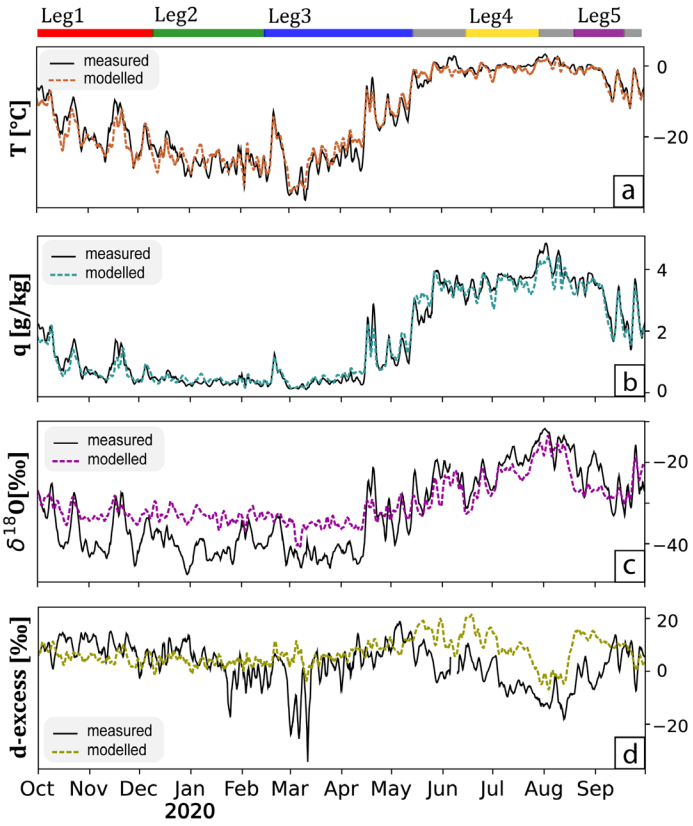

Figure 5: Time series (from 1 October 2019 to 30 September 2020) of ECHAM6-wiso model results of the nearest surface grid box, and observations along the track of RV Polarstern during MOSAiC. The subplots report modelled and measured a) air temperature (°C); b) water vapour specific humidity (g kg^{-1}); c) water vapour $\delta^{18}O$ (‰) and d) water vapour d-excess (‰). All values are averaged over a moving window of 48h.

Despite the good agreement of the specific humidity values, larger discrepancies are found between modelled and measured water vapour isotopes. For $\delta^{18}O$ (Fig. 5c), ECHAM6-wiso overestimates the absolute values of $\delta^{18}O$ in winter and early spring (Oct-April) by 6.8‰ (mean difference of the 6 h aggregated datasets). Between mid-April and end of June modelled $\delta^{18}O$ values match the measured ones. In summer (July-Sept) the simulated values are lower than the observations, with an average bias of 2.9‰. For d-excess (Fig 5d), simulated values are lower at the beginning of the winter season (Oct-Jan), but higher at the end of the winter (mid-Jan to mid-March). Modelled and measured d-excess values match between mid-March and mid-May. Modelled values are then systematically higher between mid-May and September (mean difference of 12.4‰).

The relationships between modelled and measured $\delta^{18}O$ and d-excess values for summer (JJA) and winter (DJF) are illustrated in detail in Figure 6. In summer, the correlation between modelled and observed $\delta^{18}O$ is r^2=0.70, with a slope of 0.82‰ ‰$^{-1}$, and a negative intercept of -7‰. Similarly, d-excess has a correlation of r^2=0.62, slope of 0.86‰ ‰$^{-1}$ and intercept of 12‰.

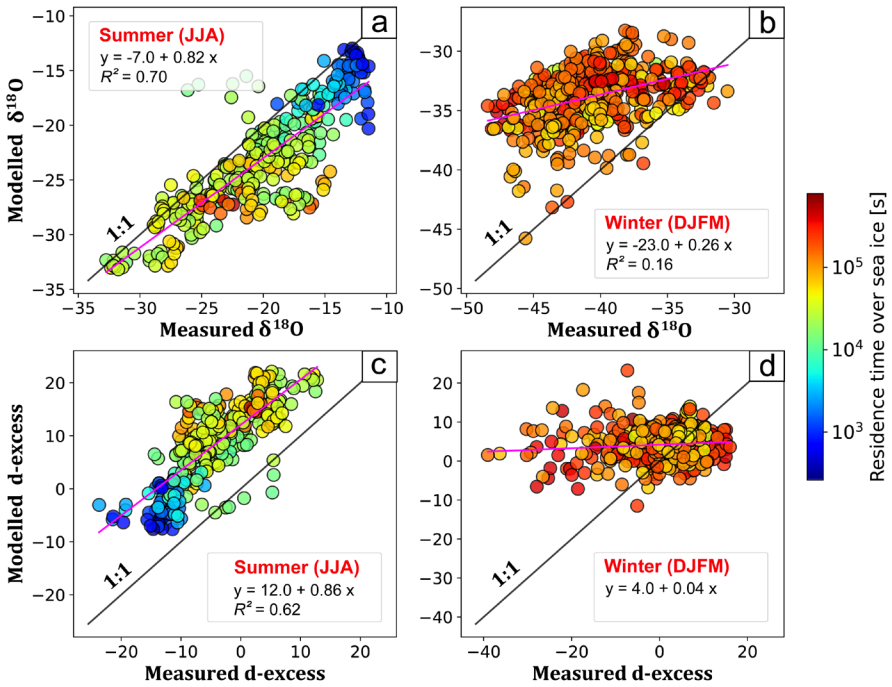

Figure 6: Seasonal scatterplots illustrating the relationships between measured and modelled $\delta^{18}O$ (a,b) and d-excess (c,d) in summer (JJA, left) and winter (DJFM, right) respectively. The data are aggregated at 6 h time resolution and they are coloured in logarithmic scale based on the residence time (s) over sea-ice retrieved from the 10-day FLEXPART backward trajectories. Linear regressions are shown as pink solid lines.

In winter, modelled and observed $\delta^{18}O$ display statistically significant but low correlation (r^2=0.16), and a slope of 0.26 ‰ ‰$^{-1}$. No correlation is observed for d-excess. In this season, the ECHAM6-wiso model is not able to reproduce neither the relative changes nor the absolute values of the isotopic measurements. To note, while residence time over the sea-ice during summer was on average 0.35 days (max: 5.6, min: 0), during winter the average residence time was 1.92 days (max 9.5, min:0.23).

4. Discussion

4.1 Correlation of measured $\delta^{18}O$ variations with local temperature and humidity changes

For the measured $\delta^{18}O$ variations in vapour on board of RV Polarstern (POL), linear relationships are found with both the observed local temperature (R^2=0.82) and specific humidity (R^2=0.88) (Figure 7). The slope between vapour $\delta^{18}O$ and temperature is 0.74‰ °C^{-1} when considering the full dataset (Fig. 7a). This relationship is not stable through the year: winter (DJF) values have a lower slope (0.42‰ °C^{-1}, R^2=0.31), while the summer (JJA) slope is steeper (1.34‰ °C^{-1}, R^2=0.57). The $\delta^{18}O$ versus temperature slope over the full record is higher than the ones observed in Ny-Ålesund (0.62 ‰ °C^{-1}, Leroy-DosSantos et al., 2020), at Invituut, in Southern Greenland (0.37 ‰ °C^{-1}, Bonne et al., 2014) and in Siberia, at the Lena River delta (0.44 ‰ °C^{-1}, Bonne et al., 2020). These latter relationships are comparable to the slope of our winter observations. The low latitude of Invituut, and the prevailing dominant weather systems were invoked as a potential explanation for such a low slope, but the comparably low slopes observed at the Lena delta and along the drifting track of MOSAiC suggest that latitude-related processes are not key controls of the temperature-isotope sensitivity. The summer

observations from MOSAiC display the steepest linear slope ever observed in the region (1.34‰ °C^{-1}), close to the one retrieved in north-western Greenland during three consecutive summers (1.1‰ °C^{-1}; Steen-Larsen et al., 2013). A shift towards higher $\delta^{18}O$ values is observed across the 0°C. This threshold marks the transition from a sublimate to an evaporative mode, where mixed phases of frozen and liquid water co-exist. The different fractionation factors associated with phase changes between these multiple compartments (e.g., open ocean, melt ponds, snow; Majoube 1971; Merlivat and Jouzel, 1979; Ellehoj et al., 2013, Lamb et al., 2017) might be responsible for the large variations of $\delta^{18}O$ observed around 0°C.

A linear relationship is also observed between $\delta^{18}O$ and the local specific humidity (R^2=0.88, slope 6.3‰ (g/kg)$^{-1}$; Fig. 7b). Here, the winter observations sampled in the Central Arctic have a rather low correlation (R^2=0.31) due to the compressed range of humidity conditions and high variability in the isotope observations. The correlation increases in summer (R^2=0.64), as the POL drifted southward in the Greenland Sea. In contrast to previous studies from the region (Leroy-Dos Santos et al., 2020, Bonne et al., 2020, Bastrikov et al., 2014), our observations do not show a logarithmic relationship with the local specific humidity. Such logarithmic relationship would agree with a theoretical Rayleigh isotopic distillation of air mass evaporating at midlatitudes and transported to high latitudes (Gat, 1996). Thus, our dataset suggests that either the air masses did not experience intense distillation processes along their trajectories or the air masses underwent local recharge of moisture modifying the isotopic composition or mixing ratio.

From this comparison of $\delta^{18}O$ versus local temperature and humidity, our data indicate that, while local temperature and local humidity are drivers of isotopic changes in summer, this is only moderately the case in winter, when the data show a weaker relationship with both temperature and specific humidity. This suggests that source or transport processes, independent of local air conditions, may contribute to influence the winter $\delta^{18}O$ signal measured at POL.

4.2 Measured d-excess changes in vapour and corresponding $\delta^{18}O$ variations

4.2.1 D-excess variations with respect to previous observations

The measured d-excess values on board POL showed a large temporal variation during the period of the MOSAiC campaign. Especially the very low, negative d-excess values measured in both winter and summer seasons are remarkable (Fig.2 and Chapter 3.1). We cannot completely rule out measurement artefacts, especially for very low humidity conditions in winter (see supplements, Text S2 for details). We also note that our d-excess values are considerably lower than previous observations from the region. For example, a 4.5 year-long monitoring of atmospheric water vapour at Ny-Ålesund revealed an average d-excess of 14.0+-7.4 ‰ (Leroy-Dos Santos et al., 2020). However, such very low negative d-excess values have not only been measured in vapour by the Picarro CRDS, but also in snow samples taken in the vicinity of POL during the MOSAiC expedition (Mellat et al., 2022). Furthermore, negative d-excess values in Arctic water vapour have been reported before: Bastrikov et al. (2014) associated negative d-excess values to mixing of dew-fall and canopy liquids with the atmospheric water vapour. This mechanism does not apply to our Central Arctic dataset, though. Steen-Larsen et al., (2013) used a 1-d box model to attribute negative d-excess values in Icelandic water vapour (as low as -10‰) to an evaporative flux into an ideally isolated planetary boundary layer above the ocean. More recently, studies from controlled laboratory and field experiments (Hughes et al., 2021) reported negative d-excess values in snow as a result of non-equilibrium exchange processes with the atmosphere. Yet, quantitative transfer functions linking

snow and vapour are still missing and there is no consensus on the physical mechanisms that could result in such negative d-excess values in the atmospheric water vapour. Finally, condensation in supersaturated conditions, which occurs at low temperature, leads to strong non-equilibrium fractionation during vapour deposition onto the ice crystal and also leads to low d-excess in the remaining vapour (Bolot et al., 2013, Dütsch et al., 2019). Given the important role played by diffusivity in water phase transitions during the formation of ice and mixed-phase clouds (Rogers, 1979), d-excess is also sensitive to in-cloud microphysical parameters such as freezing temperatures and degree of supersaturation (Samuels-Crow et al., 2014).

4.2.2 D-excess variations with respect to $\delta^{18}O$ changes

The negative d-excess values during the MOSAiC expedition are observed in two distinct seasons: in wintertime characterized by extremely dry and cold conditions and in summertime at the maximum of humidity and temperature levels (Figure 7c). Hence, there exists an anticorrelation between d-excess and $\delta^{18}O$ in summer, but a positive correlation in winter. An anticorrelation was also documented in Southern Greenland (Bonne et al., 2014), where a warm and moist summer was characterized by $\delta^{18}O$ maxima and d-excess minima. This relationship has been interpreted as the result of changes in the location of the moisture source region. Warm and moist events, with high $\delta^{18}O$ and low d-excess, were associated with moisture originating at low latitudes such as south of Greenland, as opposed to the moisture coming from the Iceland Sea or Davis Strait, characterized by lower $\delta^{18}O$ and higher d-excess. On the other hand, the measured positive correlation between $\delta^{18}O$ and d-excess during MOSAiC in winter is in agreement with the positive correlation observed by Leroy-Dos Santos et al. (2020). In this study, the authors investigated synoptic wet events during winter at Ny-Ålesund and found that the isotopic signature of moisture originating from Arctic sources is generally marked by maxima in both $\delta^{18}O$ and d-excess. According to these conclusions, seasonal changes in the moisture source could thus explain the opposite correlation observed in winter and in summer in our dataset. Yet, the positive correlation observed during winter in our dataset is largely driven by the extreme low d-excess values observed during the coldest and driest periods, so this correlation should be taken with caution with respect to measurement artefacts.

It remains open which processes are most relevant for the observed changing relationship between $\delta^{18}O$ and d-excess. Shifts in moisture origin, Rayleigh distillation along the transport pathway, deposition/condensation under supersaturated conditions during transport, deposition of vapour onto the snow surface, and snow sublimation into the atmosphere are all plausible mechanisms in play for modulating the seasonal variability of our $\delta^{18}O$ and d-excess measurements. However, it can be assumed that these processes exert varying degrees of influence during the different seasons and POL positions with respect to the sea-ice margin, with kinetic fractionation associated to evaporation and sublimation dominating in summer in proximity to the open ocean, and deposition/condensation under supersaturated conditions prevailing in winter over the sea-ice.

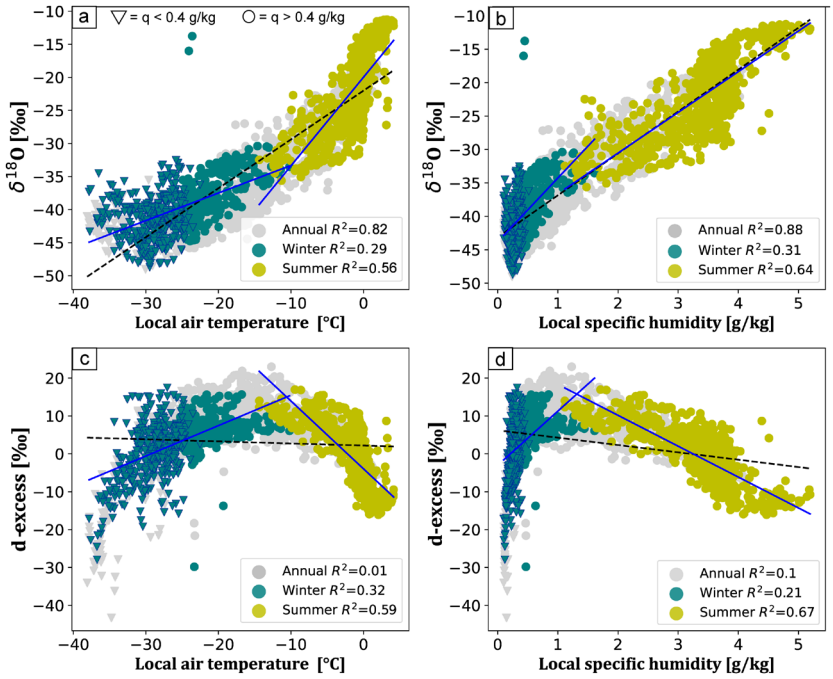

Figure 7: Scatterplots of water vapour $\delta^{18}O$ (top) and d-excess (bottom) versus local air temperature (left) and local specific humidity (right), here aggregated at 3 h resolution. The annual dataset (Oct 2019-Sept 2020) is displayed in grey, summer (JJA) values are coloured in light green and winter (DJF) values in teal. Values retrieved in humidity conditions lower than 0.4 g kg^{-1} are marked as triangles, else as circles. The linear regression line for the annual dataset is illustrated as a black dashed line; seasonal linear regressions in blue.

4.3 Linking measured d-excess changes to evaporative conditions at the moisture source

From the moisture source analyses (Sec. 3.3) we conclude that changes in moisture uptake regions are likely to modulate the sensitivity of the water vapour isotopes to both local and regional temperature. In summer, the highest evaporation rates occurred from the ice-free ocean surface and the largest contribution is identified near POL, suggesting proximal moisture uptake. In accordance, the results from the FLEXPART analysis reveal low residence time of the related air masses over sea-ice and land. Thus, changes in temperature and humidity conditions over the oceanic moisture uptake regions determine the changes in the isotopic signature of vapour at POL, without strong interference from air mass transformation during the advection. We conclude that air masses sampled during summer preserved the isotopic composition of vapour associated to primary evaporation from nearby ocean waters. During winter on the other hand, the moisture sources of the air masses were in general much more distant from POL. The backward trajectories reveal high residence times over ocean and sea-ice and, to a minor extent, over Siberia, for such transport pathways. The extended residency of air masses over sea-ice, along with the correlation of stable water isotopes to surface temperature in the ice-covered region, together suggest an influence of moisture exchange processes over the sea-ice area.

To further test this hypothesis, we examine the relationship between d-excess and the meteorological conditions in the source regions. We computed the weighted averages of T2m and Q2m from ERA5, based on the moisture uptake values retrieved from the trajectory-based moisture source diagnostic

(Sec. 3.3). To do so, a weight has been assigned to each uptake location according to its contribution to the total moisture uptake in a given time step, and a weighted average of the meteorological quantities was computed. We obtained time series of meteorological conditions at the total evaporative source, hereafter referred as T_{source} and Q_{source}, which we correlated with the local observations at POL (Figure 8). Panels a, b show the relationship of the d-excess observations and T_{source} and Q_{source}, respectively. Changes in d-excess correlate to source conditions in summer, but not in winter. During summer, the relationship with source temperature does not differ greatly from the one obtained with local temperature. The slope of d-excess and T_{source} is -1.4‰ °C^{-1}, slightly lower than -1.8‰ °C^{-1} for T_{local}. However, for Q_{source}, the slope is -4.4‰ (g/kg)$^{-1}$, half the one obtained for Q_{local} -8.15‰ (g/kg) $^{-1}$. Hence, d-excess has a higher sensitivity to local humidity.

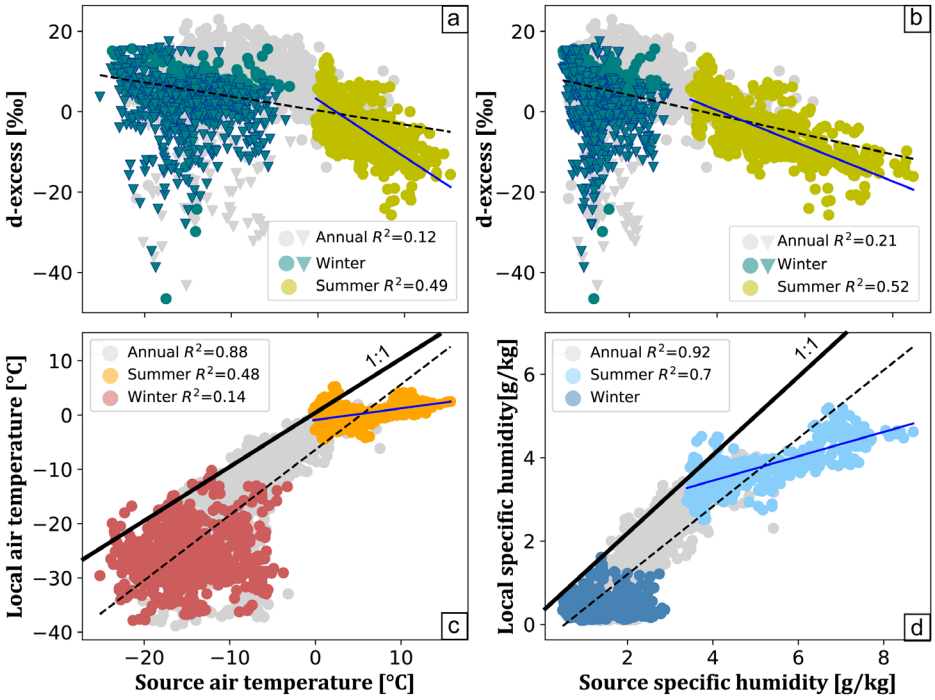

Figure 8: Upper panels: scatterplots of atmospheric water vapour d-excess and air temperature (a) and specific humidity (b) averaged over the moisture uptake regions. Lower panels: scatterplots of local and source air temperature (c) and specific humidity (d). The local meteorological data are obtained from the weather station operated onboard Polarstern, the source meteorological data are obtained from the ERA5 reanalyses from ECMWF. All datasets are aggregated at 3 h time resolution. Regression lines for the annual datasets are illustrated as a dashed black line while regression lines for the summer values are illustrated by the blue solid line.

To investigate the covariance of local and source temperature and humidity conditions, we compared Q_{source} and T_{source} to Q_{local} and T_{local} (Figure 8c, d). In summer, when moisture uptake takes place all over the Arctic basin, including coastal regions, we observe a positive correlation between the local and source variables. However, the regression line deviates from the 1:1 line and the final slopes are 0.21 and 0.30 for temperature and humidity, respectively. While T_{source} spans a variability range of ~15°C, T_{local} remains relatively constrained around 0°C. The correlation between local and source temperature conditions over summer is only slightly lower than the correlation observed between water vapour d-excess and source temperatures. These findings suggest that the influence of source conditions alone accounts for only a minor portion of the variations in d-excess. However, the relative

595 changes in evaporative temperature and humidity persist throughout the distillation pathway of the
596 air masses.
597 In contrast, during winter, we find no correlation between local and source conditions (Fig. 8c, d), or
598 between measured d-excess and T_{source} or Q_{source} (Fig. 8a, b). These results support our hypothesis of
599 air mass transformation during advection to the Central Arctic in winter time. Similarly to the air
600 mass transformation dynamics described in Thurnherr et al. (2021), where warm sectors of
601 extratropical cyclones experience net moisture loss due to dew deposition over the relatively colder
602 ocean and due to the formation of clouds in ascending air parcels, we postulate that during winter,
603 moisture loss over the Arctic sea-ice, under kinetic conditions, overprints the isotopic signal
604 associated with evaporative source conditions. Given the small amount of moisture originating at the
605 evaporative site (Barents Sea) and the long transport distance to reach the sampling location, the
606 final isotopic composition of vapour reaching POL might reflect the integrated influence of moisture
607 exchange under supersaturated conditions, such as during ice-cloud formation or solid deposition
608 onto the sea-ice. This hypothesis gains support from (i) the spatial correlation analysis (Fig. 3), where
609 winter vapour isotopes mostly display correlation with the ambient conditions over sea-ice covered
610 regions; (ii) by the moisture uptake analyses (Fig. 4d), where the trajectories of the air masses span
611 hundreds of kilometres over sea-ice covered regions.
612
613 *4.3.1 Linkage to source SST and RHskin*
614 During summer, we obtain a negative correlation of measured d-excess values with the sea surface
615 temperatures of the moisture uptake regions (slope -1.2‰ $°C^{-1}$, R^2= 0.45, Fig. S4a), but no correlation
616 is found with RH_{skin} (Fig. S4b). Anticorrelation between water vapour d-excess and RH_{sst} at source
617 was documented by Pfahl and Wernli (2008) in the Mediterranean basin, and was also observed in
618 the Atlantic and the Southern Ocean (Thurnherr et al. 2021, Bonne et al., 2019, Uemura et al., 2008).
619 This relationship describes the out of equilibrium fractionation during evaporation from the open
620 ocean (Craig and Gordon, 1965) and highlights the role of the relative humidity gradient within the
621 air column at the evaporation site. We do not have a conclusive explanation to reconcile our
622 observations to the previous datasets. The link between d-excess to evaporative source conditions
623 remains to be proven in the Central Arctic and our results suggests that this relationship may not be
624 easy to assess where moisture sources include extensive land and sea-ice covered regions.
625
626
627 *4.4 Inferences from the ECHAM6-wiso simulation results*
628
629 In the previous model version ECHAM5-wiso, systematically too high $\delta^{18}O$ values were found in the
630 Arctic region compared to near-surface vapour isotope measurements by Bonne et al. (2019). The
631 authors identified the sublimation of snow deposited on top of sea-ice as an important process
632 depleting the isotopic composition of near-surface vapour. They proposed a parameterisation of the
633 isotopic composition of the snow layer on sea-ice, which depends on the isotopic composition of the
634 snowfall. This new parameterisation, which was missing in ECHAM5-wiso and is now implemented
635 in ECHAM6-wiso (Cauquoin and Werner, 2021), might have contributed to the good match between
636 measured and modelled $\delta^{18}O$ changes in summer 2020, although it may also be responsible for an
637 over-correction as the values are now slightly too depleted (Figure 6). Despite the deviation from the
638 1:1-line, correlation values and slopes suggest that for Arctic summer conditions the ECHAM6-wiso
639 model successfully reproduces local evaporation processes and related isotope fractionation at the
640 location of POL.

Concerning d-excess, a prominent mismatch between modelled and observed values occurs in the transition between winter and spring (Fig.2, Figure S5). In this period, the most negative d-excess values (as low as -33.5‰) of the entire dataset are observed, whereas ECHAM6-wiso simulates positive d-excess values, up to 20‰. This mismatch is associated to a synoptic condition, characterized by the coldest and driest weeks of the entire sampling campaign, during which no moisture uptake was identified and a maximum residence time over sea-ice was detected. We hypothesize that during this time, the air masses underwent intense distillation under supersaturated conditions along their transport, resulting in both low $\delta^{18}O$ and d-excess values. Further, atmospheric stability (instability) is typically associated with a stratified (unstable) lower atmosphere where the snow surface is warmer (colder) than the air above, leading to positive (negative) latent heat flux in form of sublimation (deposition) between near-surface atmospheric water vapour and surface snow. Insights about potential surface moisture exchange processes will arise from the investigation of isotopic relationships between water vapour and the snow discrete samples collected during MOSAiC (Mellat et al., 2022, Macfarlane et al., 2021). More detailed process-based studies, with a focus on hoar formation and fog might also provide key insights into the coupling between air masses and sea-ice. The description of the processes leading to negative d-excess values is expected to remain partly speculative due to the uncertainties associated with our negative d-excess measurements. For future campaigns, we strongly advocate for implementing dedicated technical solutions (Leroy DosSantos, 2021) to increase instrumental accuracy at very low humidity levels (<400 ppmv).

In addition to these specific explanations for the found model-data discrepancies, there are a few more model deficits worth mentioning. The current ECHAM6-wiso model version has proven to reproduce high-resolution temporal isotopic variations well (Cauquoin and Werner 2021), however some interactions between the cryosphere and atmosphere could still be improved. E.g., no fractionation during sublimation is considered in ECHAM6-wiso, despite recent studies observing kinetic fractionation during snow post-depositional processes (Casado et al., 2018) and during sublimation of snow to the atmosphere (Wahl et al., 2021, 2022). Furthermore, the isotopic parameterisation of precipitation under supersaturation conditions is tuned to match the observed Antarctic snow, without evidence that this relationship may be representative of the Arctic region (Dütsch et al., 2019). Moreover, our ECHAM6-wiso simulation setup prescribes the sea-ice coverage from ERA5 data which do not account for the presence of melt ponds and leads. The influence of such small open water bodies on the isotope signal of water vapour is still subject to debate. Klein et al. (2016) argued that sea-ice extent primarily acts on the distillation path depleting the air masses and causing strong kinetic fractionation during evaporation from local sources such as leads and polynyas. Whether these small-scale processes indeed can have a cumulative effect and an imprint on the near-surface water vapour at the regional scale remains to be demonstrated. High-resolution gridded datasets of lead fraction (Melsheimer & Spreen, 2019) and melt ponds (Webster et al., 2022) might be used in future ECHAM6-wiso studies to prescribe the presence of liquid water on the sea-ice. In addition, numerical modelling of isotope fractionation at the snow-air interphase will provide a first-order understanding on the role of the cryosphere to impact the water vapour at the regional and seasonal scale, especially in winter. Coupled simulations of AGCMs with a complex snowpack model enabled for water isotopes fractionation (CROCUS, Touzeau et al., 2018) might also allow an improved assessment of the contributions of such processes in the Arctic realm.

5. Conclusions

During the MOSAiC drifting campaign, we operated an autonomous water vapour isotope analyser onboard the research vessel Polarstern (POL). In this study, we present the atmospheric water vapour isotopes measurements, spanning an entire annual cycle from October 2019 to September 2020. We observed a seasonal cycle in water vapour $\delta^{18}O$, which mimics the seasonal changes in local temperature and humidity. The isotopic composition of the summer moisture correlates with surface temperature and humidity over the ocean sector and the margin of the sea-ice, while winter moisture is associated to changes in near-surface conditions over the sea-ice. To investigate whether these differences are a consequence of different moisture origin, we combine isotopic measurements with a moisture source analysis, based on semi-Lagrangian back-trajectory simulations. During the summer season, we observed significant moisture uptake in proximity to the sampling site, at the margin of the retreating sea-ice. The environmental conditions at these evaporative sites correlate with those at the location of POL, and with the water vapour d-excess signal. Thus, we infer that during summer the water vapor isotopes retain valuable information about source temperature and humidity. In contrast, winter moisture sampled during MOSAiC originated over the sea-ice-free region of the Barents Sea. This is an important finding, in consideration that the Barents Sea has undergone severe sea-ice loss in recent decades and may act as a progressively more prominent source of winter moisture for the Arctic realm. However, we found no correlation between evaporative source conditions and the d-excess signal measured in the water vapour onboard POL. Results from an isotope-enabled ECHAM6-wiso simulation indicate that evaporative processes from the open ocean and distillation along the transport (under isotopic equilibrium conditions) are not sufficient to explain our observations. We suggest that non-equilibrium isotopic fractionation processes during the transport over sea-ice, beyond what is currently included in the used ECHAM6-wiso atmosphere model, are key to modulating the d-excess values in Arctic moisture in winter. Considering the uncertainties in the parameterization of kinetic fractionation in supersaturated conditions, we advocate for future sensitivity studies to assess the isotopic signature associated to ice or mixed-phase clouds, as well as solid deposition on the snow surface under supersaturated conditions.

This study delivers a baseline for understanding Arctic moisture origin and transport pathways in the current warming climate. However, it also carries a high level of complexity due to the spatiotemporal variability of the signal acquired along a drifting track and the uncertainties associated with both the isotopic measurements and the moisture source diagnostics in extremely cold and dry conditions. Yet, as the understanding of the Arctic water cycle and the ability to model its future change is limited by the paucity of observations, our dataset of stable water isotope observations can serve as a unique benchmark to test the sensitivity of climate models and their parameterisation.

Open Research

The calibrated near-surface atmospheric water vapour isotopes measurements (Brunello et al., 2022a, b,c,d,e) and the continuous meteorological surface measurements (Schmithüsen 2021a, b,c,d,e) obtained during the MOSAiC campaign are published in the data repository PANGEA. This study uses ERA5 hourly data at the surface (Hersbach et al., 2023), available at Copernicus Climate Change Service, Climate Data Store. The ECHAM6-wiso simulation (Cauquoin and Werner, 2021) was performed at the Alfred Wegener Institute supercomputing centre. The ECHAM model code is

available under a version of the MPI-M software license agreement. The code of the isotopic version ECHAM6-wiso is available upon request on AWI's GitLab repository.

Acknowledgements

The authors declare no real or perceived financial conflicts of interests in regard of this work. The data used in this manuscript were produced as part of the international Multidisciplinary drifting Observatory for the Study of the Arctic Climate (MOSAiC) with the tag MOSAiC20192020. We thank all those who contributed to MOSAiC and made this endeavour possible (Nixdorf et al. 2021). This study was carried out as part of the project "Changes of water isotopes in Arctic Sea-ice, Ocean and atMosphere" (CiASOM), which received support from the German Federal Ministry of Education and Research (BMBF, award no. 03F0869A). The authors acknowledge the assistance of J.-L. Bonne, S. Bagheri and M. Behrens for the design, set up and support regarding the custom-designed calibration module. We thank J. Welker and B. Kopec for the helpful discussions about atmospheric transport pathways across the Arctic region.

References

Aemisegger, F. (2018). On the link between the North Atlantic storm track and precipitation deuterium excess in Reykjavik. *Atmospheric Science Letters, 19*(12). doi: 10.1002/asl.865

Bailey, H., Hubbard, A., Klein, E. S., Mustonen, K. R., Akers, P. D., Marttila, H., & Welker, J. M. (2021). Arctic sea-ice loss fuels extreme European snowfall. *Nature Geoscience, 14*(5), 283-+. doi:10.1038/s41561-021-00719-y

Bastrikov, V., Steen-Larsen, H. C., Masson-Delmotte, V., Gribanov, K., Cattani, O., Jouzel, J., & Zakharov, V. (2014). Continuous measurements of atmospheric water vapour isotopes in western Siberia (Kourovka). *Atmospheric Measurement Techniques, 7*(6), 1763-1776. doi:10.5194/amt-7-1763-2014

Bengtsson, L., Hodges, K. I., Koumoutsaris, S., Zahn, M., & Keenlyside, N. (2011). The changing atmospheric water cycle in Polar Regions in a warmer climate. *Tellus Series a-Dynamic Meteorology and Oceanography, 63*(5), 907-920. doi:10.1111/j.1600-0870.2011.00534.x

Berkelhammer, M., Noone, D. C., Wong, T. E., Burns, S. P., Knowles, J. F., Kaushik, A., . . . Williams, M. W. (2016). Convergent approaches to determine an ecosystem's transpiration fraction. *Global Biogeochemical Cycles, 30*(6), 933-951. doi:10.1002/2016gb005392

Bintanja, R. (2018). The impact of Arctic warming on increased rainfall. *Scientific Reports, 8*. doi:10.1038/s41598-018-34450-3

Bintanja, R., & Selten, F. M. (2014). Future increases in Arctic precipitation linked to local evaporation and sea-ice retreat. *Nature, 509*(7501), 479-+. doi:10.1038/nature13259

Bolot, M., Legras, B., & Moyer, E. J. (2013). Modelling and interpreting the isotopic composition of water vapour in convective updrafts. Atmospheric Chemistry and Physics, 13(16), 7903-7935.

Bonne, J. L., Behrens, M., Meyer, H., Kipfstuhl, S., Rabe, B., Schönicke, L., . . . Werner, M. (2019). Resolving the controls of water vapour isotopes in the Atlantic sector. *Nat Commun, 10*(1), 1632. doi:10.1038/s41467-019-09242-6

Bonne, J. L., Masson-Delmotte, V., Cattani, O., Delmotte, M., Risi, C., Sodemann, H., & Steen-Larsen, H. C. (2014). The isotopic composition of water vapour and precipitation in Ivittuut, southern

Greenland. *Atmospheric Chemistry and Physics, 14*(9), 4419-4439. doi:10.5194/acp-14-4419-2014

Bonne, J. L., Meyer, H., Behrens, M., Boike, J., Kipfstuhl, S., Rabe, B., . . . Werner, M. (2020). Moisture origin as a driver of temporal variabilities of the water vapour isotopic composition in the Lena River Delta, Siberia. *Atmospheric Chemistry and Physics, 20*(17), 10493-10511. doi:10.5194/acp-20-10493-2020

Bonne, J. L., Steen-Larsen, H. C., Risi, C., Werner, M., Sodemann, H., Lacour, J. L., . . . Masson-Delmotte, V. (2015). The summer 2012 Greenland heat wave: In situ and remote sensing observations of water vapor isotopic composition during an atmospheric river event. *Journal of Geophysical Research-Atmospheres, 120*(7), 2970-2989. doi:10.1002/2014jd022602

Breant, C., Dos Santos, C. L., Agosta, C., Casado, M., Fourre, E., Goursaud, S., . . . Landais, A. (2019). Coastal water vapor isotopic composition driven by katabatic wind variability in summer at Dumont d'Urville, coastal East Antarctica. *Earth and Planetary Science Letters, 514*, 37-47. doi:10.1016/j.epsl.2019.03.004

Brunello, Camilla F; Werner, Martin; Meyer, Hanno; Mellat, Moein; Bonne, Jean-Louis (2022a): Continuous near-surface atmospheric water vapour isotopic composition from Polarstern cruise PS122-1 (MOSAiC). PANGAEA, https://doi.org/10.1594/PANGAEA.951424

Brunello, Camilla F; Werner, Martin; Meyer, Hanno; Mellat, Moein; Bonne, Jean-Louis (2022b): Continuous near-surface atmospheric water vapour isotopic composition from Polarstern cruise PS122-2 (MOSAiC). PANGAEA, https://doi.org/10.1594/PANGAEA.951446

Brunello, Camilla F; Werner, Martin; Meyer, Hanno; Mellat, Moein; Bonne, Jean-Louis (2022c): Continuous near-surface atmospheric water vapour isotopic composition from Polarstern cruise PS122-3 (MOSAiC). PANGAEA, https://doi.org/10.1594/PANGAEA.951447

Brunello, Camilla F; Werner, Martin; Meyer, Hanno; Mellat, Moein; Bonne, Jean-Louis (2022d): Continuous near-surface atmospheric water vapour isotopic composition from Polarstern cruise PS122-4 (MOSAiC). PANGAEA, https://doi.org/10.1594/PANGAEA.951448

Brunello, Camilla F; Werner, Martin; Meyer, Hanno; Mellat, Moein; Bonne, Jean-Louis (2022e): Continuous near-surface atmospheric water vapour isotopic composition from Polarstern cruise PS122-5 (MOSAiC). PANGAEA, https://doi.org/10.1594/PANGAEA.951449

Butzin, M., Werner, M., Masson-Delmotte, V., Risi, C., Frankenberg, C., Gribanov, K., . . . Zakharov, V. I. (2014). Variations of oxygen-18 in West Siberian precipitation during the last 50 years. *Atmospheric Chemistry and Physics, 14*(11), 5853-5869. doi:10.5194/acp-14-5853-2014

Casado, M., Landais, A., Picard, G., Münch, T., Laepple, T., Stenni, B., . . . Jouzel, J. (2018). Archival processes of the water stable isotope signal in East Antarctic ice cores. *The Cryosphere, 12*(5), 1745-1766. doi:10.5194/tc-12-1745-2018

Casado, M., Landais, A., Picard, G., Arnaud, L., Dreossi, G., Stenni, B., & Prié, F. (2021). Water isotopic signature of surface snow metamorphism in Antarctica. Geophysical Research Letters, 48(17), e2021GL093382

Cauquoin, A., & Werner, M. (2021). High-Resolution Nudged Isotope Modeling With ECHAM6-Wiso: Impacts of Updated Model Physics and ERA5 Reanalysis Data. *Journal of Advances in Modeling Earth Systems, 13*(11). doi:e2021MS00253210.1029/2021MS002532

Cauquoin, A., Werner, M., & Lohmann, G. (2019). Water isotopes - climate relationships for the mid-Holocene and preindustrial period simulated with an isotope-enabled version of MPI-ESM. *Climate of the Past, 15*(6), 1913-1937. doi:10.5194/cp-15-1913-2019

Cohen, J., Screen, J. A., Furtado, J. C., Barlow, M., Whittleston, D., Coumou, D., ... & Jones, J. (2014). Recent Arctic amplification and extreme mid-latitude weather. Nature geoscience, 7(9), 627-637.

Cohen, J., Zhang, X., Francis, J., Jung, T., Kwok, R., Overland, J., . . . Yoon, J. (2020). Divergent consensuses on Arctic amplification influence on midlatitude severe winter weather. *Nature Climate Change, 10*(1), 20-+. doi:10.1038/s41558-019-0662-y

Craig, H. (1961). Isotopic Variations in Meteoric Waters. *Science, 133*(3465), 1702-1703. doi:10.1126/science.133.3465.1702

Craig, H., & Gordon, L. I. (1965). Deuterium and oxygen 18 variations in the ocean and the marine atmosphere.

Dansgaard, W. (1964). Stable isotopes in precipitation. tellus, 16(4), 436-468.

Dutsch, M., Blossey, P. N., Steig, E. J., & Nusbaumer, J. M. (2019). Nonequilibrium Fractionation During Ice Cloud Formation in iCAM5: Evaluating the Common Parameterization of Supersaturation as a Linear Function of Temperature. *Journal of Advances in Modeling Earth Systems, 11*(11), 3777-3793. doi:10.1029/2019ms001764

Dutsch, M., Pfahl, S., & Wernli, H. (2016). Drivers of delta H-2 variations in an idealized extratropical cyclone. *Geophysical Research Letters, 43*(10), 5401-5408. doi:10.1002/2016gl068600

Ellehoj, M. D., Steen-Larsen, H. C., Johnsen, S. J., & Madsen, M. B. (2013). Ice-vapor equilibrium fractionation factor of hydrogen and oxygen isotopes: experimental investigations and implications for stable water isotope studies. *Rapid Commun Mass Spectrom, 27*(19), 2149-2158. doi:10.1002/rcm.6668

Fremme, A. and Sodemann, H. (2019), The role of land and ocean evaporation on the variability of precipitation in the Yangtze River valley, Hydrol. Earth Syst. Sci., 23, 2525-2540, 2019 https://doi.org/10.5194/hess-23-2525-2019

Gat, J. R. (1996). Oxygen and hydrogen isotopes in the hydrologic cycle. *Annual Review of Earth and Planetary Sciences, 24*, 225-262. doi:DOI 10.1146/annurev.earth.24.1.225

Graham, R. M., Hudson, S. R., & Maturilli, M. (2019). Improved Performance of ERA5 in Arctic Gateway Relative to Four Global Atmospheric Reanalyses. *Geophysical Research Letters, 46*(11), 6138-6147. doi:10.1029/2019gl082781

Hersbach, H., Bell, B., Berrisford, P., Biavati, G., Horányi, A., Muñoz Sabater, J., Nicolas, J., Peubey, C., Radu, R., Rozum, I., Schepers, D., Simmons, A., Soci, C., Dee, D., Thépaut, J-N. (2023): ERA5 hourly data on single levels from 1940 to present. Copernicus Climate Change Service (C3S) Climate Data Store (CDS), DOI: 10.24381/cds.adbb2d47

Hoffmann, G., Werner, M., & Heimann, M. (1998). Water isotope module of the ECHAM atmospheric general circulation model: A study on timescales from days to several years (vol 103, pg 16871, 1998). *Journal of Geophysical Research-Atmospheres, 103*(D18), 23323-23323. Retrieved from <Go to ISI>://WOS:000076302900024

Holland, M. M., & Bitz, C. M. (2003). Polar amplification of climate change in coupled models. *Climate Dynamics, 21*(3-4), 221-232. doi:10.1007/s00382-003-0332-6

Hu, J., Yan, Y. Z., Yeung, L. Y., & Dee, S. G. (2022). Sublimation Origin of Negative Deuterium Excess Observed in Snow and Ice Samples From McMurdo Dry Valleys and Allan Hills Blue Ice Areas, East Antarctica. *Journal of Geophysical Research-Atmospheres, 127*(11). doi:e2021JD03595010.1029/2021JD035950

Huang, J. B., Zhang, X. D., Zhang, Q. Y., Lin, Y. L., Hao, M. J., Luo, Y., . . . Zhang, J. S. (2017). Recently amplified arctic warming has contributed to a continual global warming trend. *Nature Climate Change, 7*(12), 875-+. doi:10.1038/s41558-017-0009-5

867 Hughes, A. G., Wahl, S., Jones, T. R., Zuhr, A., Horhold, M., White, J. W. C., & Steen-Larsen, H. C. (2021).
868 The role of sublimation as a driver of climate signals in the water isotope content of surface
869 snow: laboratory and field experimental results. *Cryosphere, 15*(10), 4949-4974.
870 doi:10.5194/tc-15-4949-2021
871 Jouzel, J., & Merlivat, L. (1984). Deuterium and oxygen 18 in precipitation: Modeling of the isotopic
872 effects during snow formation. Journal of Geophysical Research: Atmospheres, 89(D7),
873 11749-11757.
874 Klein, E. S., & Welker, J. M. (2016). Influence of sea ice on ocean water vapor isotopes and Greenland
875 ice core records. *Geophysical Research Letters, 43*(24), 12475-12483.
876 doi:10.1002/2016gl071748
877 Kopec, B. G., Feng, X., Posmentier, E. S., & Sonder, L. J. (2019). Seasonal Deuterium Excess Variations
878 of Precipitation at Summit, Greenland, and their Climatological Significance. *Journal of*
879 *Geophysical Research-Atmospheres, 124*(1), 72-91. doi:10.1029/2018jd028750
880 Kopec, B. G., Feng, X. H., Michel, F. A., & Posmentier, E. S. (2016). Influence of sea ice on Arctic
881 precipitation. *Proceedings of the National Academy of Sciences of the United States of*
882 *America, 113*(1), 46-51. doi:10.1073/pnas.1504633113
883 Kurita, N. (2011). Origin of Arctic water vapor during the ice-growth season. *Geophysical Research*
884 *Letters, 38*(2), n/a-n/a. doi:10.1029/2010gl046064
885 Lamb, K. D., Clouser, B. W., Bolot, M., Sarkozy, L., Ebert, V., Saathoff, H., ... & Moyer, E. J. (2017).
886 Laboratory measurements of HDO/H2O isotopic fractionation during ice deposition in
887 simulated cirrus clouds. Proceedings of the National Academy of Sciences, 114(22), 5612-
888 5617.
889 Leroy-Dos Santos, C., Casado, M., Prie, F., Jossoud, O., Kerstel, E., Farradeche, M., . . . Landais, A.
890 (2021). A dedicated robust instrument for water vapor generation at low humidity for use
891 with a laser water isotope analyzer in cold and dry polar regions. *Atmospheric Measurement*
892 *Techniques, 14*(4), 2907-2918. doi:10.5194/amt-14-2907-2021
893 Leroy-Dos Santos, C., Masson-Delmotte, V., Casado, M., Fourré, E., Steen-Larsen, H. C., Maturilli, M., . .
894 . Landais, A. (2020). A 4.5 Year-Long Record of Svalbard Water Vapor Isotopic Composition
895 Documents Winter Air Mass Origin. *Journal of Geophysical Research: Atmospheres, 125*(23).
896 doi:10.1029/2020jd032681
897 Majoube, M. (1971). Fractionnement en oxygène 18 et en deutérium entre l'eau et sa vapeur.
898 Journal de Chimie Physique, 68, 1423-1436.
899 Macfarlane, Amy R; Schneebeli, Martin; Dadic, Ruzica; Wagner, David N; Arndt, Stefanie; Clemens-
900 Sewall, David; Hämmerle, Stefan; Hannula, Henna-Reetta; Jaggi, Matthias; Kolabutin,
901 Nikolai; Krampe, Daniela; Lehning, Michael; Matero, Ilkka; Nicolaus, Marcel; Oggier, Marc;
902 Pirazzini, Roberta; Polashenski, Chris; Raphael, Ian; Regnery, Julia; Shimanchuck, Egor;
903 Smith, Madison M; Tavri, Aikaterini (2021): Snowpit raw data collected during the MOSAiC
904 expedition. PANGAEA, https://doi.org/10.1594/PANGAEA.935934
905 Mellat, Moein; Meyer, Hanno; Brunello, Camilla F; Arndt, Stefanie; Macfarlane, Amy R; Schneebeli,
906 Martin; Hörhold, Maria; Werner, Martin; Weiner, Mikaela; Marent, Andreas (2022): Stable
907 water isotopes of snow during MOSAiC expedition. PANGAEA,
908 https://doi.org/10.1594/PANGAEA.948511
909 Melsheimer, Christian; Spreen, Gunnar (2019): AMSR2 ASI sea ice concentration data, Arctic,
910 version 5.4 (NetCDF) (July 2012 - December 2019). PANGAEA,
911 https://doi.org/10.1594/PANGAEA.898399
912 Merlivat, L. (1978). Molecular Diffusivities of (H2o)-O-1 6 Hd16o, and (H2o)-O-18 in Gases. *Journal*
913 *of Chemical Physics, 69*(6), 2864-2871. doi:Doi 10.1063/1.436884

914 Merlivat, L., & Jouzel, J. (1979). Global Climatic Interpretation of the Deuterium-Oxygen-18
915 Relationship for Precipitation. *Journal of Geophysical Research-Oceans, 84*(Nc8), 5029-5033.
916 doi:DOI 10.1029/jc084ic08p05029
917 Pisso, I., Sollum, E., Grythe, H., Kristiansen, N. I., Cassiani, M., Eckhardt, S., Arnold, D., Morton, D.,
918 Thompson, R. L., Groot Zwaaftink, C. D., Evangeliou, N., Sodemann, H., Haimberger, L.,
919 Henne, S., Brunner, D., Burkhart, J. F., Fouilloux, A., Brioude, J., Philipp, A., Seibert, P., and
920 Stohl, A.: The Lagrangian particle dispersion model FLEXPART version 10.4, Geosci. Model
921 Dev., 12, 4955–4997, https://doi.org/10.5194/gmd-12-4955-2019, 2019
922 Pfahl, S., & Wernli, H. (2008). Air parcel trajectory analysis of stable isotopes in water vapor in the
923 eastern Mediterranean. *Journal of Geophysical Research-Atmospheres, 113*(D20).
924 doi:D2010410.1029/2008jd009839
925 Polarstern: Alfred-Wegener-Institut Helmholtz-Zentrum für Polar- und Meeresforschung. (2017).
926 Polar Research and Supply Vessel POLARSTERN Operated by the Alfred-Wegener-Institute.
927 Journal of large-scale research facilities, 3, A119. http://dx.doi.org/10.17815/jlsrf-3-163.
928 Rinke, A., Cassano, J. J., Cassano, E. N., Jaiser, R., & Handorf, D. (2021). Meteorological conditions
929 during the MOSAiC expedition. *Elementa: Science of the Anthropocene, 9*(1).
930 doi:10.1525/elementa.2021.00023
931 Ritter, F., Steen-Larsen, H. C., Werner, M., Masson-Delmotte, V., Orsi, A., Behrens, M., . . . Kipfstuhl, S.
932 (2016). Isotopic exchange on the diurnal scale between near-surface snow and lower
933 atmospheric water vapor at Kohnen station, East Antarctica. *Cryosphere, 10*(4), 1647-1663.
934 doi:10.5194/tc-10-1647-2016
935 Rogers, R. R., & Yau, M. K. A short course in cloud physics. Bull. Amer. Meteor. Soc, 45, 619.
936 Samuels-Crow, K. E., Galewsky, J., Sharp, Z. D., & Dennis, K. J. (2014). Deuterium excess in
937 subtropical free troposphere water vapor: Continuous measurements from the Chajnantor
938 Plateau, northern Chile. Geophysical Research Letters, 41(23), 8652-8659.
939 Schmithüsen, Holger (2021a): Continuous meteorological surface measurement during
940 POLARSTERN cruise PS122/1. Alfred Wegener Institute, Helmholtz Centre for Polar and
941 Marine Research, Bremerhaven, PANGAEA, https://doi.org/10.1594/PANGAEA.935221
942 Schmithüsen, Holger (2021b): Continuous meteorological surface measurement during
943 POLARSTERN cruise PS122/2. Alfred Wegener Institute, Helmholtz Centre for Polar and
944 Marine Research, Bremerhaven, PANGAEA, https://doi.org/10.1594/PANGAEA.935222
945 Schmithüsen, Holger (2021c): Continuous meteorological surface measurement during
946 POLARSTERN cruise PS122/3. Alfred Wegener Institute, Helmholtz Centre for Polar and
947 Marine Research, Bremerhaven, PANGAEA, https://doi.org/10.1594/PANGAEA.935223
948 Schmithüsen, Holger (2021d): Continuous meteorological surface measurement during
949 POLARSTERN cruise PS122/4. Alfred Wegener Institute, Helmholtz Centre for Polar and
950 Marine Research, Bremerhaven, PANGAEA, https://doi.org/10.1594/PANGAEA.935224
951 Schmithüsen, Holger (2021e): Continuous meteorological surface measurement during
952 POLARSTERN cruise PS122/5. Alfred Wegener Institute, Helmholtz Centre for Polar and
953 Marine Research, Bremerhaven, PANGAEA, https://doi.org/10.1594/PANGAEA.935225
954 Serreze, M. C., & Barry, R. G. (2011). Processes and impacts of Arctic amplification: A research
955 synthesis. *Global and Planetary Change, 77*(1-2), 85-96.
956 doi:10.1016/j.gloplacha.2011.03.004
957 Shupe, M. D., Rex, M., Blomquist, B., Persson, P. O. G., Schmale, J., Uttal, T., . . . Yue, F. G. (2022).
958 Overview of the MOSAiC expedition-Atmosphere INTRODUCTION. *Elementa-Science of the*
959 *Anthropocene, 10*(1). doi:110.1525/elementa.2021.00060

960 Sodemann, H., Schwierz, C., & Wernli, H. (2008). Interannual variability of Greenland winter
961 precipitation sources: Lagrangian moisture diagnostic and North Atlantic Oscillation
962 influence. Journal of Geophysical Research: Atmospheres, 113(D3).
963 Sodemann, H., and A. Stohl (2009), Asymmetries in the moisture origin of Antarctic precipitation,
964 Geophys. Res. Lett., 36, L22803, doi:10.1029/2009GL040242.
965 Steen-Larsen, H. C., Johnsen, S. J., Masson-Delmotte, V., Stenni, B., Risi, C., Sodemann, H., . . . White, J.
966 W. C. (2013). Continuous monitoring of summer surface water vapor isotopic composition
967 above the Greenland Ice Sheet. *Atmospheric Chemistry and Physics, 13*(9), 4815-4828.
968 doi:10.5194/acp-13-4815-2013
969 Steen-Larsen, H. C., Sveinbjornsdottir, A. E., Jonsson, T., Ritter, F., Bonne, J. L., Masson-Delmotte, V., . .
970 . Vinther, B. M. (2015). Moisture sources and synoptic to seasonal variability of North
971 Atlantic water vapor isotopic composition. *Journal of Geophysical Research-Atmospheres,*
972 *120*(12), 5757-5774. doi:10.1002/2015jd023234
973 Stevens, B., Giorgetta, M., Esch, M., Mauritsen, T., Crueger, T., Rast, S., . . . Roeckner, E. (2013).
974 Atmospheric component of the MPI-M Earth System Model: ECHAM6. *Journal of Advances in*
975 *Modeling Earth Systems, 5*(2), 146-172. doi:10.1002/jame.20015
976 Stohl, A., Forster, C., Frank, A., Seibert, P., & Wotawa, G. (2005). Technical note: The Lagrangian
977 particle dispersion model FLEXPART version 6.2. *Atmospheric Chemistry and Physics, 5*,
978 2461-2474. doi:DOI 10.5194/acp-5-2461-2005
979 Thurnherr, I., Kozachek, A., Graf, P., Weng, Y., Bolshiyanov, D., Landwehr, S., . . . Aemisegger, F.
980 (2020). Meridional and vertical variations of the water vapour isotopic composition in the
981 marine boundary layer over the Atlantic and Southern Ocean. *Atmospheric Chemistry and*
982 *Physics, 20*(9), 5811-5835. doi:10.5194/acp-20-5811-2020
983 Thurnherr, I., Hartmuth, K., Jansing, L., Gehring, J., Boettcher, M., Gorodetskaya, I., ... & Aemisegger,
984 F. (2021). The role of air–sea fluxes for the water vapour isotope signals in the cold and
985 warm sectors of extratropical cyclones over the Southern Ocean. Weather and Climate
986 Dynamics, 2(2), 331-357.
987 Touzeau, A., Landais, A., Morin, S., Arnaud, L., & Picard, G. (2018). Numerical experiments on vapor
988 diffusion in polar snow and firn and its impact on isotopes using the multi-layer energy
989 balance model Crocus in SURFEX v8.0. *Geoscientific Model Development, 11*(6), 2393-2418.
990 doi:10.5194/gmd-11-2393-2018
991 Uemura, R., Matsui, Y., Yoshimura, K., Motoyama, H., & Yoshida, N. (2008). Evidence of deuterium
992 excess in water vapor as an indicator of ocean surface conditions. *Journal of Geophysical*
993 *Research-Atmospheres, 113*(D19). doi:D19114 10.1029/2008jd010209
994 Urey, H. C. (1947). The thermodynamic properties of isotopic substances. *Journal of the Chemical*
995 *Society* (Resumed), 562-581. doi: 10.1039/JR9470000562
996 Vihma, T., Screen, J., Tjernstrom, M., Newton, B., Zhang, X. D., Popova, V., . . . Prowse, T. (2016). The
997 atmospheric role in the Arctic water cycle: A review on processes, past and future changes,
998 and their impacts. *Journal of Geophysical Research-Biogeosciences, 121*(3), 586-620.
999 doi:10.1002/2015jg003132
1000 Wahl, S., Steen-Larsen, H. C., Reuder, J., & Horhold, M. (2021). Quantifying the Stable Water
1001 Isotopologue Exchange Between the Snow Surface and Lower Atmosphere by Direct Flux
1002 Measurements. *Journal of Geophysical Research-Atmospheres, 126*(13). doi:e2020JD034400
1003 10.1029/2020JD034400
1004 Wang, C. X., Graham, R. M., Wang, K. G., Gerland, S., & Granskog, M. A. (2019). Comparison of ERA5
1005 and ERA-Interim near-surface air temperature, snowfall and precipitation over Arctic sea

ice: effects on sea ice thermodynamics and evolution. *Cryosphere, 13*(6), 1661-1679. doi:10.5194/tc-13-1661-2019

Werner, M., Langebroek, P. M., Carlsen, T., Herold, M., & Lohmann, G. (2011). Stable water isotopes in the ECHAM5 general circulation model: Toward high-resolution isotope modeling on a global scale. *Journal of Geophysical Research-Atmospheres, 116*. doi:D1510910.1029/2011jd015681

Ye, K. H., & Messori, G. (2021). Inter-model spread in the wintertime Arctic amplification in the CMIP6 models and the important role of internal climate variability. *Global and Planetary Change, 204*. doi:10354310.1016/j.gloplacha.2021.103543

Zahn, M., Akperov, M., Rinke, A., Feser, F., & Mokhov, I. I. (2018). Trends of Cyclone Characteristics in the Arctic and Their Patterns From Different Reanalysis Data. *Journal of Geophysical Research-Atmospheres, 123*(5), 2737-2751. doi:10.1002/2017jd027439

Zhang, X. D., He, J. X., Zhang, J., Polyakov, I., Gerdes, R., Inoue, J., & Wu, P. L. (2013). Enhanced poleward moisture transport and amplified northern high-latitude wetting trend. *Nature Climate Change, 3*(1), 47-51. doi:10.1038/Nclimate1631

Webster MA, Holland M, Wright NC, Hendricks S, Hutter N, et al. (2022). Spatiotemporal evolution of melt ponds on Arctic sea ice: MOSAiC observations and model results. Elem Sci Anth 10(1): 000072.